In-Plane and Out-of-Plane Constraint Effects in Three-Dimensional Elastic Perfectly-Plastic Crack Tip Fields

Feizal Yusof and J. W. Hancock
Department of Mechanical Engineering, University of Glasgow, Glasgow, G12 8QQ, UK

ABSTRACT

The structure of three-dimensional crack tip fields under elastic perfectly–plastic conditions has been examined using three-dimensional boundary layer formulations following Nakamura and Parks [1, 2]. The remote boundary conditions were based on the first two terms of the Williams [3] expansion of the elastic plane stress field. The asymptotic stresses at the crack tip were determined by extrapolation along radial lines to show the crack tip field as a function of load level and thickness. On the mid-plane, a plane strain field develops which is retained even when the radius of the plastic zone is greater than the plate thickness. As the free surface is approached out–of-plane constraint is lost, and an elastic-perfectly plastic corner field is attained rather than a plane stress field, due to through thickness stress gradients near the free surface. The three-dimensional fields are compared with elastic perfectly–plastic fields developed for the limiting two-dimensional cases of plane strain and plane stress.

1. INTRODUCTION

The structure of fully three-dimensional crack tip fields is fundamental to fracture mechanics. The problem has been usefully simplified into the important limiting cases of plane strain and plane stress deformation. Under plane strain deformation a family of crack tip fields which depend upon constraint have been identified by Du and Hancock [4]. The fields depend upon the T-stress, which is the first non-singular term in the Williams [2] expansion. Positive T-stresses allow the development of the fully constrained Prandtl field which is the limit of the HRR fields in the limit of non-hardening plasticity. Negative (compressive) T-stresses cause a loss of constraint, through a family of deviatorically similar but hydrostatically different crack tip fields. Crack tip constraint may be lost due to either in-plane effects associated with non-singular crack tip terms (Betegon and Hancock [5], O'Dowd and Shih [6]), or by out-of-plane effects associated with the finite thickness of a test specimen and deviations from plane strain conditions. Under elastic perfectly-plastic conditions the plane stress field has been discussed by Sham and Hancock [7]. The present work addresses constraint loss in the full three-dimensional problem, which combines constraint loss effects due to in-plane effects and out-of plane effects, under conditions in which the plastic zone is small compared to the in-plane dimensions, but allowed to vary with respect to the plate thickness, and thus fall outside the ASTM [8] limits for small scale yielding.

2. NUMERICAL METHODS

Crack tip plasticity in a finite thickness plate has been studied by modelling the near tip domain as a circular disk with a radial through thickness crack as shown in Figure 1. Both right handed Cartesian (x_1, x_2, x_3) and cylindrical (z, r, θ) co-ordinate systems centred at the crack tip are used, such that a straight crack front is located on the x_3-axis, and the crack flanks lie along on the (x_2 = 0) plane. The radius to thickness ratio of the disk ensured that the radius of the plastic zone was small compared to in plane dimensions, while enabling plasticity to develop over scales which were allowed to become large compared to the plate thickness. Under mode I loading the problem has reflective symmetry with respect to both the mid-plane (x_3 = 0) and the crack plane (x_2 = 0),

allowing the geometry to be represented by a symmetric quarter that was modelled with first order eight noded brick, as illustrated in Figure 2. The elements were focused at the crack tip while maintaining a constant angular span of 10^0. An identical mesh structure was repeated along the crack front from the mid-plane ($x_3 = 0$) to the free surface ($x_3/t = 1/2$), refining the mesh toward the free surface.

At the crack tip element, aspect ratios capable of giving reliable numerical results were developed using two levels of sub-structuring, as illustrated in Figure 2. An outer-mesh, with a radius to thickness ratio (r/t) of 100 modelled the overall configuration. The outer-mesh comprised 360 elements arranged as a single layer of 20 circumferential rings of 18 elements. Displacement boundary conditions corresponding to a mode I plane stress crack-tip stress field were imposed on the outer perimeter using the mode I stress intensity factor K as a loading parameter, allowing the out of plane displacement u_3 to remain a free variable.

$$u_1 + iu_2 = \frac{K}{2G}\left(\frac{r}{2\pi}\right)^{1/2} (\kappa - \cos(\theta)) e^{i\theta/2} \quad (1)$$

Here G is the shear modulus, and $\kappa = (3 - \upsilon)/(1 + \upsilon)$ for plane stress, where υ is Poisson's ratio. The outer elastic field was checked against the corresponding plane stress field to be of the form:

$$\sigma_{ij} = \frac{K}{\sqrt{2\pi r}} f_{ij}(\theta) \quad (2)$$

where f_{ij} are universal functions of angle (θ). To achieve mesh refinement in both the radial and through thickness directions, displacements from the outer mesh were interpolated to nodes on the outer boundary of an intermediate mesh. This comprised 1350 elements disposed in 5 layers through the half thickness, (t /2). The intermediate mesh was further sub-structured to a near-tip mesh, which was designed to provide accurate solutions of field variables near the crack front. The near tip mesh consisted of 7776 elements in 16 layers through the half thickness, the radial extent of the near tip mesh being close to 5t. The crack tip was modelled with 18 rings of 8 noded tri-linear hexahedron elements collapsed to give 19 coincident but independent nodes at the tip. The near tip was resolved with elements having a radius of 5t/1000, while the field at the intersection of the crack front with the free surface was identified using an element thickness of t/1000.

Two–dimensional plane strain and plane stress crack tip fields were established using two-dimensional boundary layer formulations (Rice and Tracey [10]) without sub-structuring.

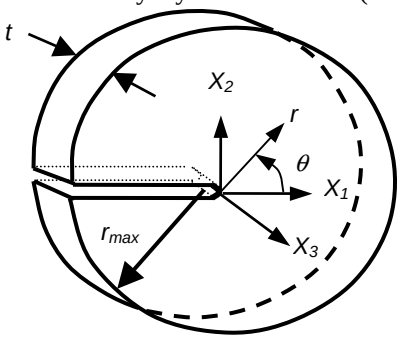

Figure 1: Circular Disk representing a thin plate.

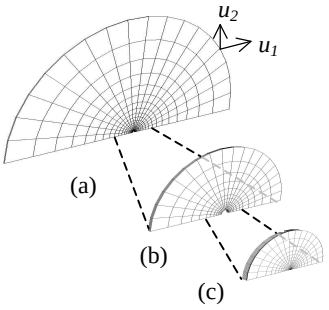

Figure 2 (a), (b), (c): FE model of Outer, Intermediate, and Near Tip mesh respectively.

The material response was idealised as elastic perfectly-plastic, with a uniaxial yield stress σ_o and a corresponding tensile strain ε_0. At stresses less than the yield stress ($\sigma \le \sigma_o$) a homogenous isotropic elastic response was adopted using a Poisson ratio 0.49, which results in close to incompressible deformation. The stress-strain relation was generalised for multi-axial stress states of stress using the Mises yield criterion and an associated flow rule to describe incremental

plasticity within a framework of small strain deformation. The modified B-bar method discussed by Nakamura et al. [11] was used to stabilise the model against spurious pressure modes.

The applied load is quantified by the non-dimensional loading parameter $J_{far}/\sigma_0\varepsilon_0$ where J_{far} , J-integral at the outer boundary, was determined from the applied stress intensity factor K . Local value of the J-integral along the crack front was determined by domain integral methods implemented in ABAQUS [9]. The local T-stress along the crack front was determined under elastic conditions by an interaction integral method described by Nakamura and Parks [12] as implemented in ABAQUS [9].

3. RESULTS

Although the remote loading is uniform, the intensity of the loading may vary along the crack front as quantified by the local values of the J-integral, J_{local}. Figure 3 shows J_{local} along the crack front at four load levels, $J_{far}/\sigma_0\varepsilon_0$ = 1, 3, 5, 8. The local values of J are amplified over the remotely applied value of J near the mid-plane but attenuated near the free surface.

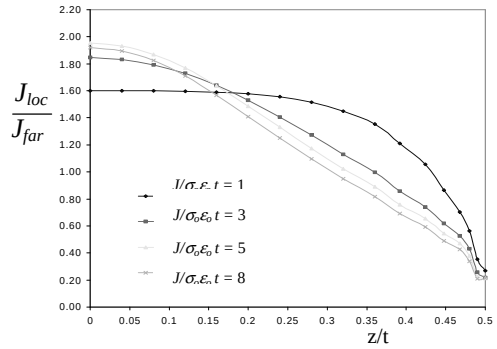

Figure 3: Local J normalised by remote J, along half-crack front at load levels: 1, 3, 5, 8.

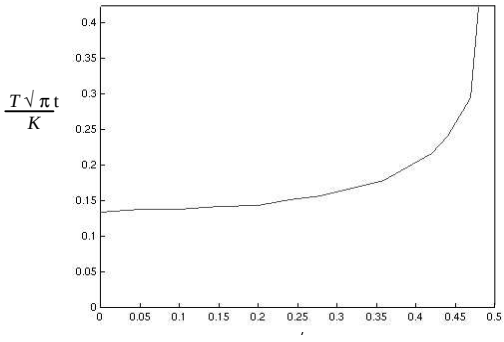

Figure 4: Variation of T-stress along the crack front in a thin elastic plate with Poisson's ratio = 0.49

The variation in the local T-stress along the crack front in a thin elastic plate is shown in Figure 4. Even if no T-stress is applied in the remote field, the configuration develops an inherently positive (tensile) T-stress that increases markedly towards the free surface. It is therefore necessary to distinguish between a the local values of the T-stress and that in the remote boundary layer field, $T_{applied}$. The proximity to plane strain conditions along the crack front can be quantified by an out of plane constraint parameter $\sigma_{zz}/(\sigma_{\theta\theta} + \sigma_{r\theta})$ that is shown in Figure 5. In incompressible plane strain deformation this parameter is 0.5 and approaches zero as proximity to plane strain is lost. On the mid-plane this parameter approaches 0.5 indicating that the deformation is close to plane strain conditions but decays with distance from the mid-plane and the crack tip as shown in Figure 5.

The development of plasticity depends on the local variation in J and the constraint along the crack front. On the centre plane the plastic zone shape is similar to the two-dimensional plane stress field. The development of plasticity at the free surface is illustrated in Figure 6, in which absolute distances are non-dimensionalised by J_{local}/σ_0. Initially the free surface plastic zone shape is distinctly different, although it recovers the plane stress shape at higher levels of deformation as the plastic zone becomes larger than the plate thickness.

Under elastic-perfectly plastic deformation the crack tip stresses are finite, and were obtained by extrapolating to the tip along radial lines at 10^o intervals using a post processing routine. The crack tip stresses for the three-dimensional field in which loading is only based on the stress intensity factor ($T_{applied}$ = 0) are shown in Figures 7 and 8

.

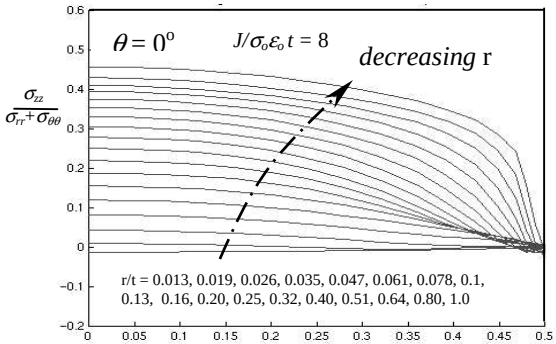

Figure 5: Out of plane of plane constraint parameter at load level 8.

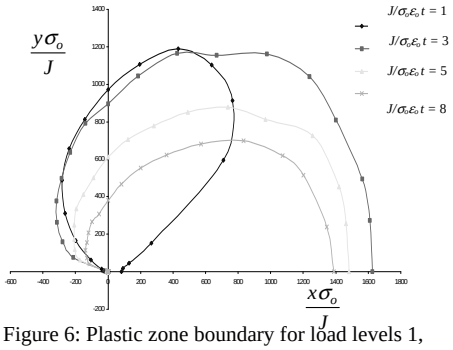

Figure 6: Plastic zone boundary for load levels 1, 3. 5. 8 at z/t = 0.5

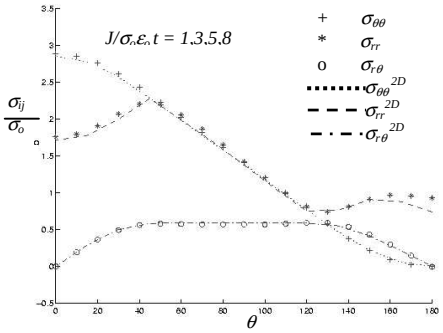

Figure 7: Cylindrical stresses for 3D non hardening, at z/t =0. (T = 0) solution at z/t =0

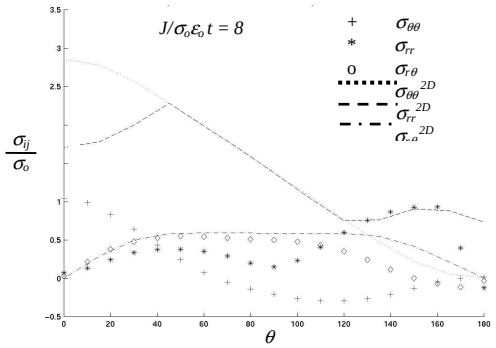

Figure 8: Cylindrical stresses for 3D non hardening solution at z/t = 0.5, (T = 0)

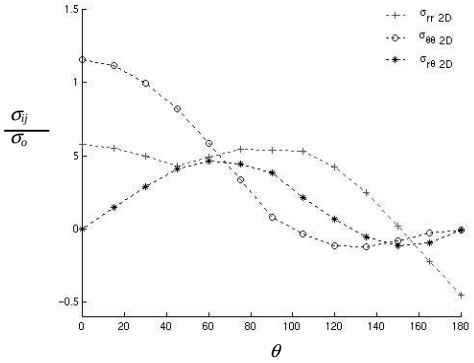

Figure 9: Cylindrical stresses for the 2D plane stress non-hardening solution.

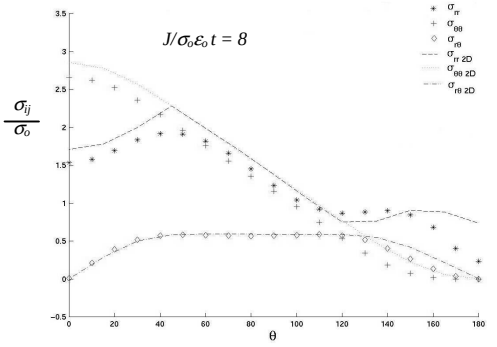

Figure 10: Cylindrical stresses for the 3D non-hardening (T = -0.5σ_0) Tapp = -0.5σ_o at a load level

Figure 7 shows the stresses on the mid-plane (z/t = 0) compared with the two-dimensional (T = 0) plane strain field, which is shown with broken lines. The stress field on the free surface (z/t =0.5) is shown in Figure 8, where it is compared to the two-dimensional (T = 0) plane strain field. It is also relevant to compare the free surface field with the two-dimensional plane stress field shown in Figure 9. Figure 10 shows the crack tip stress field for $T_{applied}$ = -0.5σ_o. The compressive T-stress results in a loss in constraint in the leading sectors of the field, paralleling the effect in the two-dimensional plane strain field.

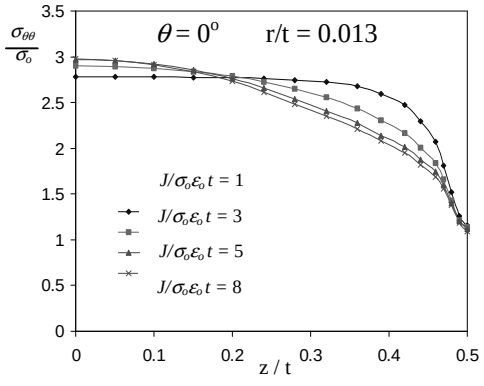

Figure 11: Normalised opening hoop stress through thickness at load levels 1, 3, 5, 8.

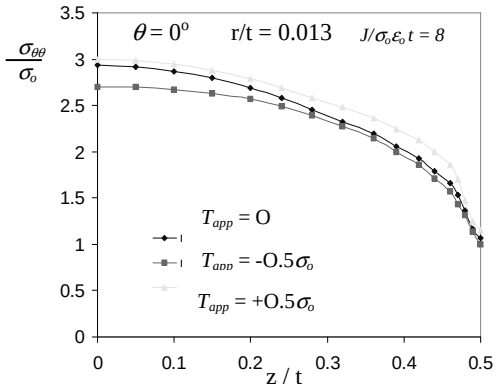

Figure 12: Normalised hoop stress for T applied = $0.5\sigma_o$, 0, $-0.5\sigma_o$.

4. DISCUSSION

It is remarkable that on the mid-plane, the three-dimensional solution is close to the two-dimensional plane strain solution, even at deformation levels of $J_{far}/\sigma_0\varepsilon_0 = 8$, when the maximum radius of the plastic zone is more than twice the plate thickness. A more detailed presentation of the hoop stress directly ahead of the crack is given in Figure 11. On the mid-plane ($z/t = 0$) the hoop stress and associated constraint initially rise with deformation. Du and Hancock [4] and Betegon and Hancock [5] have discussed the effect of the T-stress on the hoop stress and constraint level. The current configuration develops an inherently tensile (positive) T-stress, which varies along the crack front as shown in Figure 12. As the T-stress is proportional to the applied load, T is close to zero at the lowest load level ($J_{far}/\sigma_0\varepsilon_0 = 1$), and the stress field at the mid–plane corresponds to the $T = 0$, two-dimensional plane strain solution. However as the load level rises, T becomes tensile (more positive) on the mid-plane resulting in an increase in constraint, and stress levels approaching the fully constrained Prandtl field. The full three-dimensional solution also exhibits plasticity at all angles around the crack tip, which is a feature of the ($T > 0$) two-dimensional plane strain solutions. The two-dimensional ($T = 0$) plane strain field exhibits an elastic wedge on the crack flanks, which disappears when T becomes tensile and expands when T becomes compressive. This feature is also shown by the three-dimensional field when T becomes negative. Although the T-stress becomes even more markedly tensile close to the free surface the stress field here is dominated by the loss of out of plane constraint effects.

The asymptotic stress field on the free surface shown in Figure 9 may be compared to the two-dimensional plane stress field, shown in Figure 10. Plane stress requires that two condition are met:

$$\sigma_{zz} = \sigma_{rz} = \sigma_{\theta z} = 0 \qquad \frac{d\sigma_{zz}}{dz} = \frac{d\sigma_{zr}}{dz} = \frac{d\sigma_{z\theta}}{dz} = 0 \qquad (3)$$

The condition is met at the free surface. However the second set requiring that there are no stress gradients in the through thickness direction is not satisfied. Under perfectly elastic conditions this results a corner field, which does not exhibit the familiar two-dimensional $r^{-1/2}$ stress singularity, as discussed by Benthem [13]. Under perfectly-plastic conditions both the plane stress and corner fields show the familiar r^0 dependence, but the structure of the free surface field is completely different to that in plane stress. Directly ahead of the crack ($\theta = 0$), the curved fan which is a feature of the plane stress field requires that $\sigma_{\theta\theta} = 2\sigma_{rr}$ and $\sigma_{r\theta} = 0$, however directly the corner field shows ($\theta = 0$), $\sigma_{\theta\theta} = \sigma_o$, $\sigma_{rr} = \sigma_{r\theta} = 0$.

5. CONCLUSIONS

Three dimensional elastic perfectly-plastic crack tip fields in thin plates exhibit high levels of constraint, associated with near plane strain deformation even when the radius of the plastic zone is very much greater than the plate thickness. The three-dimensional configuration generates an inherently positive *T*-stress which tends to counteract the loss of constraint due to out of plane effects. However compressive applied *T*-stresses in the far field reduce constraint near the mid-plane in three-dimensional configurations in the same way that occurs in two-dimensional plane strain fields. Constraint is also lost due to out of plane effects and the departure from plane strain conditions as the free surface is approached along the crack front. The free surface field is however distinctly different to the two-dimensional plane stress field due to the significance of strong out of plane stress gradients.

6. ACKNOWLEDGEMENTS

Feizal Yusof gratefully acknowledges the fellowship from University of Science Malaysia which enabled the research to be carried out in Glasgow University. The ABAQUS finite element code was made available under academic license from Hibbitt, Karlsson and Sorensen Inc., Pawtucket, R.I.

7. REFERENCES

1. Nakamura, T., Parks, D.M. (1988). “Three-Dimensional Stress Field near the Crack Front of a Thin Elastic Plate.” Journal of Applied Mechanics, Vol. 55, pp. 805-813.
2. Nakamura, T., Parks, D.M. (1990). “Three-Dimensional Crack Front Fields in A Thin Ductile Plate.” Journal of the Mechanics and Physics of Solids, Vol. 38, No. 6, pp. 787-812.
3. Williams, M. L., (1957). “On the stress distribution at the base of a stationary crack.” ASME Journal of Applied Mechanics, Vol. 24, pp. 111-114.
4. Du, Z-Z., Hancock, JW. (1991). “The effect of non-singular stresses on crack-tip constraint”, Journal of the Mechanics and Physics of Solids, vol. 39, no. 4, pp. 555-567.
5. Betegon, C., Hancock, J.W., (1991). “Two-Parameter Characterization of Elastic-Plastic Crack-Tip fields”, Journal of Applied Mechanics, vol. 58, pp. 104-110.
6. O’Dowd N.P., Shih C. F., (1991). “A Family of crack-tip fields characterized by a triaxiality parameter: Part I – Structure of fields”. Journal of the Mechanics and Physics of Solids, Vol. 39, pp.939-963.
7. Sham, T.L., and Hancock, J. W., (1999). “Mode I crack tip fields with incomplete crack tip plasticity in plane stress.” Journal of the Mechanics and Physics of Solids, Vol. 47, pp. 2011-2027.
8. ASTM (E399-90), (1990). “Standard Test Method for Plane strain fracture toughness of metallic materials.” American Society for Testing and Materials, Philadelphia.
9. ABAQUS, (2003). Version 6.3, Hibbitt, Karlsson and Sorensen Inc., Pawtucket, RI.
10. Rice, J.R., Tracey, D.M., (1973). “Computational Fracture Mechanics”, in Numerical and Computer Methods in Structural Mechanics, edited by S. J. Fenves et al., Academic Press, New York.
11. Nakamura, T., Shih, C. F., Freund, L. B., (1986). “Analysis of a Dynamically loaded three-point-bend ductile fracture specimen.” Engineering Fracture Mechanics, Vol. 25, No. 3, pp. 323-339.
12. Nakamura T., Parks D.M., (1992). “Determination of elastic *T*-Stress along Three-Dimensional crack fronts using an Interaction Integral” Int. J. of Solids and Structures, vol. 29, no. 13, pp. 1597-1611.
13. Benthem, J.P., (1977). “State of stress at the vertex of a quarter-infinite crack in a half space,” International Journal of Solids and Structures, Vol. 13. pp. 479-492.